Vietnam Journal of Earth Sciences, 48(2), 225–244, https://doi.org/10.15625/2615-9783/23852

Vietnam Journal of Earth Sciences
https://vjs.ac.vn/index.php/jse

Wave-induced sediment dynamics and seabed changes around the Truong Sa Island, Vietnam

Nguyen Xuan Tung[1,2*], Nguyen Minh Huan[2], Nguyen Kim Cuong[2], Pham Duc Hung[1], Luc Anh Tuan[3,4]

[1]*Institute of Earth Sciences, VAST, Hanoi, Vietnam*
[2]*VNU University of Science, Vietnam National University, Hanoi*
[3]*Vietnam National University Ho Chi Minh City, Institute for Environment and Resources, Ho Chi Minh City, Vietnam*
[4]*Kyoto University, Disaster Prevention Research Institute, Uji City, Kyoto, Japan*

Received 02 April 2025; Received in revised form 14 September 2025; Accepted 29 November 2025

ABSTRACT

This study investigated wave-induced suspended sediment dynamics and seabed morphological changes around the Truong Sa Island in the East Vietnam Sea. The analysis was conducted using the MIKE 21/3 Coupled Model FM, which integrates wave, hydrodynamic, sediment transport, and bed evolution modules to simulate seabed responses to both seasonal and interannual wave forcing during 2013–2015. The model was forced with ERA5 reanalysis data and validated using observed tidal and bathymetric datasets from the Vietnam Academy of Science and Technology (VAST). Results revealed that seabed changes were most pronounced in the northeastern nearshore region of the Truong Sa Island. It was driven by the prevailing northeast-directed wave conditions, which also contributed to elevated suspended sediment concentrations (SSCs). Seasonally, winter exhibited more dynamic seabed changes and greater suspended sediment variability than summer. Under the most severe wave conditions in 2015, the simulated domain experienced a net seabed incision with an average depth of -0.54 m. Spatially, the nearshore areas were characterized by significant seabed incision and high SSCs, whereas offshore regions showed minimal seabed changes and low SSCs. Moreover, persistent sediment deposition was observed in the harbor southwest of the Truong Sa Island, implying the need for regular dredging to maintain operational capacity. The findings underscore the need for integrated management strategies that balance coastal development, marine ecosystem protection, and navigational safety.

Keywords: Wave dynamics, suspended sediment, seabed changes, MIKE21/3, Truong Sa Island, East Vietnam Sea.

1. Introduction

Oceanic islands have been developed over thousands of years through sediment contributions from rivers worldwide and through sea-level falls (Kench et al., 2022). These islands are home to millions of people, fostering diverse cultures and concentrating assets and infrastructures (Martyr-Koller et al., 2021). Small islands and their coral reefs provide valuable ecosystems for island and coastal communities (Kench and Mann, 2017). However, the environments of many islands

*Corresponding author, Email: nxtung@ies.vast.vn

have been altered (Campbell, 2018) due to climate change and anthropogenic activities (Mentaschi et al., 2018).

Climate change and anthropogenic activities have led to landform changes worldwide (Mentaschi et al., 2018), including the formation of small emergent and atoll islands (Holdaway et al., 2021). Anthropogenic activities, including dredging and land reclamation, have increasingly impacted the evolution, ecosystems, and environments of islands, particularly for geopolitical, military, economic, and livelihood purposes (Mora et al., 2016; Smith et al., 2019). On the other hand, small islands are particularly vulnerable to climate change, especially sea-level rise (Holdaway et al., 2021; Kennedy, 2024), due to their limited size, low elevation, and limited physical and economic capacity. Climate change-induced sea level rise may intensify tropical storms and storm surges (Bacmeister et al., 2018), significantly eroding small islands along their coastlines and nearshore bathymetry (Kench and Mann, 2017).

Small islands are strongly affected by global climate change-induced unfavorable weather and wave behavior (Hanich et al., 2018; Kennedy, 2024; Vousdoukas et al., 2023). Waves can overtop coastlines, increasing erosion and flood inundation susceptibility in small islands (Ford et al., 2018). Wave-induced overtopping flow can erode coastlines and the seabed, with the eroded sediment subsequently transported away by currents (Li et al., 2024). Waves affect sediment interactions among the seashore, reefs, and the far shore, thereby shaping the morphology of the nearshore seabed (Bramante et al., 2020) by eroding and transporting large sediment volumes offshore (Watson et al., 2017).

Traditionally, direct bathymetric measurements of the ocean around the islands have been effective for studying seafloor erosion and deposition, thereby enabling the identification of island-prone areas. Watson et al. (2017) used a multibeam acoustic echosounder to measure bathymetry and examine evolutionary processes at the Ontong Java and Nukumanu atolls in the Pacific Ocean. Although the results from the multibeam echosounder are highly accurate, they are costly to operate. Moreover, the measurement team may encounter unforeseen safety issues at sea, including strong waves and other extreme weather conditions. Therefore, long-term bathymetric data for islands worldwide collected with a multibeam echosounder are relatively rare. This limitation underscores the rationale for applying numerical hydrodynamic models, which offer a cost-effective and safe means of assessing seabed evolution under wave and current forcing.

Alternatively, satellites and remote sensing are effective tools for examining land changes in deltas, islands, and atolls (Binh et al., 2020; Holdaway et al., 2021; Vu et al., 2024; Nguyen et al., 2022). They have been used to map the geometry and marine habitats (Lyons et al., 2020; Dang et al., 2023), dredging activities for island building (Smith et al., 2019), and to assess ecological vulnerability (Ma et al., 2023). Remote sensing techniques are widely employed to map and analyze bathymetric changes, especially in nearshore estuaries and islands (Lyons et al., 2011). For instance, Yen et al. (2017) mapped the shallow bathymetry of the Truong Sa Island using Landsat 8 images and remote sensing techniques. Remote sensing techniques can produce reliable results in areas up to 15–20 m deep, but not in areas deeper than that (Yen et al., 2017), such as up to some hundred meters in the surroundings of many Pacific Ocean islands. Although remote sensing techniques can be used to map seafloor bathymetry, they pose challenges for examining the controlling factors of bathymetric changes. Moreover,

high-resolution satellites (e.g., Worldview and Quickbird) can provide detailed and accurate results but are costly (Han et al., 2024).

On the other hand, coarser-resolution satellites (e.g., Landsat) can be free but may be compensated for by lower accuracies and reliabilities. Additionally, free optical satellites may provide limited imagery for analysis due to cloud cover. Given the inherent limitations of field surveys and remote sensing, numerical modeling remains an effective tool in assessing the mechanisms and drivers of seabed bathymetric evolution.

As islanders largely depend on the marine environment for their livelihoods and culture (Friedlander, 2018), the erosion of bathymetry around small islands may destabilize them and lead to biodiversity loss, thereby jeopardizing livelihoods. Therefore, understanding nearshore bathymetric changes under strong wave conditions is crucial for managers to develop strategic plans and measures that sustain the islands and support the communities that underpin them. However, studies of nearshore bathymetric changes have received less attention, as most previous research has focused on shoreline movement, biodiversity, and ecosystems (Barnett and Adger, 2003; Huang et al., 2015; Wolanski et al., 2020). Although wave energy likely poses a significant threat to island instability (Storlazzi et al., 2018), the effects of waves on bathymetric and sediment dynamics still receive less attention. Consequently, changes in sediment transport and oceanic bathymetry under strong waves have not been adequately studied in the Pacific Ocean and the Spratly Islands of Vietnam.

Therefore, this research aims to (1) examine wave dynamics around the Truong Sa Island in the East Vietnam Sea, and (2) assess sediment dynamics and seabed changes under varying wave conditions. The assessments are conducted seasonally and interannually using a two-dimensional (2D) wave-dynamics, sediment-transport, and bed-evolution model. The results of this research will be valuable for island management, ensuring safe navigation, promoting livelihood sustainability, and potentially supporting ecosystem maintenance.

2. Study area

The East Vietnam Sea covers an area of over 3 million km^2, with bathymetry ranging from shallow waters to deep waters (over 5,000 m) (Huang et al., 2015). The Truong Sa Archipelago (the Spratly Islands) is located approximately 400 km off the coast of Vietnam, in Khanh Hoa Province (Fig. 1). It covers an area of 409,000-480,000 km^2 (Vu and Vu, 2024; Yen et al., 2017) and is famous for its significant marine biodiversity (Huang et al., 2015), with approximately 26 islands and over 600 coral reefs (Han et al., 2024). The Truong Sa Archipelago spans 800 km east-west and 600 km north-south. There are five main island groups, including Truong Sa, Song Tu, Nam Yet, Vinh Vien, and Tham Hiem (Yen et al., 2017). Islands in the Truong Sa Archipelago are relatively small, with nearshore elevations above the mean sea level ranging from 0.5–6 m for the emerged parts and from -90 to 0.5 m for the submerged parts. Waves vary seasonally, with the northeast and southwest being the dominant directions in the corresponding northeast and southwest monsoons.

The Truong Sa Archipelago is located in the central East Vietnam Sea, where hydrodynamic conditions are dominated by seasonal monsoons and frequently influenced by tropical typhoons. The region is affected by about 1–2 typhoons or tropical storms each year, mainly in September-November, often generating extreme winds and strong waves. The northeast monsoon (November-April) produces northeasterly waves with significant heights of 2–3 m, occasionally exceeding 3.5 m, while the southwest monsoon

(May-October) induces southwesterly waves with lower magnitudes, typically 1–2 m. Tides are semidiurnal with a moderate range (1–2 m), interacting with wind-driven currents and reef bathymetry to form complex nearshore circulation. Climate change projections indicate that wave regimes at Truong Sa are likely to change significantly (Nguyen et al., 2017).

Truong Sa Island, located in the western part of the Truong Sa Archipelago, has an elliptical shape, measuring 0.65 km^2 and stretching 4.6 km northeast-southwest by 1.5 km wide. This shape is standard among the islands and atolls in the Truong Sa Archipelago due to the region's tectonic features and monsoon circulation (Li et al., 2024). The Truong Sa Island is relatively flat, with elevations ranging from 3.4 to 5.0 m. The shore areas of the island encompass 1.21 ha (elevations from 0 to -20 m), 38.19 ha (-20 to -50 m), 45.35 ha (-50 to -100 m), and 69.42 ha (-100 to -200 m). Its shoreline is variable due to wave and current dynamics (Khuong et al., 2022). The island's sediment primarily consists of coarse sand and gravel, resulting from the destruction of coral reefs and shells.

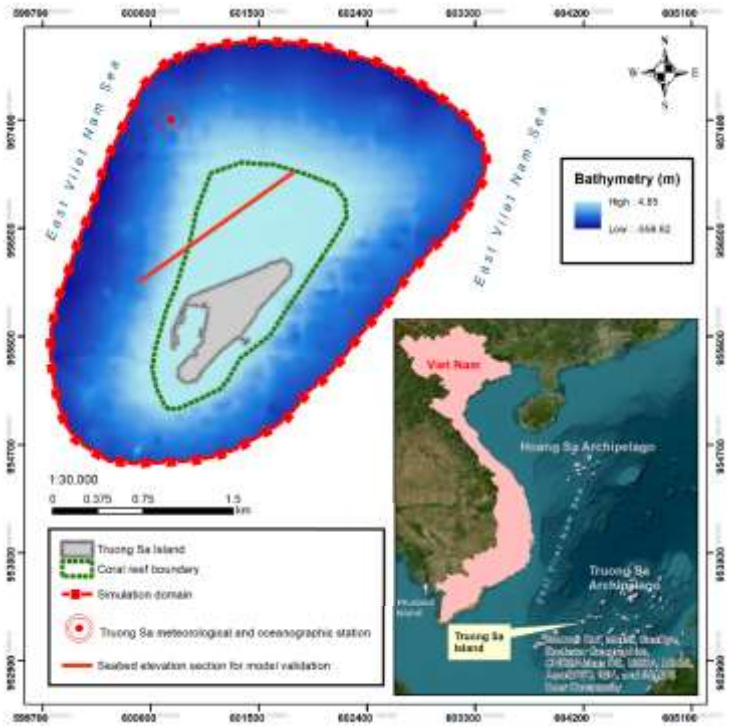

Figure 1. Map of the Truong Sa Archipelago and the Truong Sa Island, including the boundary of the numerical model, oceanographic monitoring station, and bathymetry

3. Materials and methods

3.1. General methodology

Figure 2 shows the research flowchart. First, we collected the historical wind, wave, water level, and bathymetry data. Second, we processed and analyzed the collected data before performing the analysis. Third, we established a 2D Mike 21/3 model with hydrodynamic, wave, and sediment transport modules. Fourth, the model was calibrated and validated for hydrodynamics, waves, and seabed evolution. Fifth, the validated model simulated wave regimes, sediment dynamics,

and seabed changes at the seasonal and interannual scales. Sixth, the effects of waves on sediment dynamics and seabed changes were examined. The central step of the study focused on analyzing the impact of waves on sediment dynamics and seabed changes. This included seasonal comparisons (summer vs. winter) and an interannual assessment of extreme wave years (2013–2015). Seventh, recommendations for island management, safe navigation, and coral reef sustainability were made based on the simulation results.

Figure 2. Flowchart of the research methodology

3.2. Data

Appendix 1 summarizes the datasets used in this study. We collected daily wave data from the Truong Sa Oceanographic station (Fig. 1) from 2005 to 2022, provided by the Vietnam Academy of Science and Technology (VAST). These wave data were analyzed for frequency to determine the 3-year most extreme wave conditions for numerical simulations, and the results were used to calibrate and validate the 2D wave model. Additionally, we collected ERA5 reanalysis wave data at 6-hour intervals from ECMWF (Hersbach et al., 2023) from 2013 to 2018 to serve as boundary conditions for the 2D wave model. Wind data were also collected at 6-hour intervals during 2013–2018 at the Truong Sa Oceanographic Station from VAST to support the analysis of atmospheric forcing on hydrodynamic processes in the wind module.

We collected 12-hour-interval water-level data at the Truong Sa Oceanographic gauge from 2013 to 2015 from VAST, and 6-hour-interval ERA5 reanalysis water-level data from the ECMWF (Hersbach et al., 2023) from 2013 to 2018. The ECMWF reanalysis data were used as boundary conditions for the 2D model, whereas the gauged data were used to calibrate and validate the hydrodynamic model. Both wave and water-level raster data from ECMWF had a spatial resolution of 0.5 × 0.5° (Hersbach et al., 2023).

We collected the seabed bathymetry data for 2010 and 2018 from VAST. The 2010 and 2018 datasets were in point format, with spatial intervals of 100 m and 300 m, respectively. The 2010 bathymetric survey was conducted using a single-beam echo sounder (accuracy ±0.1 m), while the 2018 survey used a multibeam echo sounder (accuracy ±0.05 m) under calm sea conditions. To consolidate the two datasets, both were standardized to the same vertical national datum and interpolated into a standard grid before model input. The 2010 bathymetric data were used to establish the computational geometric data for the 2D model, whereas the 2018 bathymetric data were used to validate the established model.

3.3. Wave frequency analysis to determine the simulation period

Daily wave data from the Truong Sa oceanographic station from 2005 to 2022 were used to calculate annual 1-day and 90-day maximum values using the Indicators of Hydrologic Alteration software version 7.1 (The Nature Conservancy, 2009). We then determined three continuous years with the most severe significant wave height based on these two wave indicators (i.e., 1-day and

90-day maxima) to numerically simulate the effects of severe waves on seabed bathymetry. The 1-day and 90-day data were used because they represent the most severe short and long-term wave conditions. We found that the three consecutive years 2013–2015 had the highest wave heights, ranging from 3.5 m to 3.83 m for the 1-day maximum and from 1.2 m to 1.35 m for the 90-day maximum (Appendix 2). Therefore, we established a 2D Mike 21/3 model to simulate the effects of waves on hydrodynamics, sediment dynamics, and seabed changes from 2013 to 2015.

3.4. Two-dimensional hydrodynamic, wave, and sediment transport model

We utilized the MIKE 21/3 Coupled Model FM, which employs an unstructured finite-element mesh, to examine wave-driven influences on hydrodynamics, sediment transport, and seabed morphology around Truong Sa Island. This modelling framework employs a dynamic coupling approach to simulate the interactions between waves, currents, sediment, and seabed evolution. The hydrodynamic and spectral wave modules form the computational backbone of the model, generating essential flow and wave conditions that drive sediment transport simulations (DHI, 2014). In this study, we applied the MIKE 21/3 Coupled Model FM (a widely used commercial model) in 2-D mode, which is computationally efficient and well-suited to the available datasets.

The sand transport module in the coupled model calculates sediment transport rates, including bed load and suspended load, continuously throughout the simulation. These calculations use either empirical or theoretical transport equations, shown in the following equations (Lu et al., 2020; van Rijn, 1984):

$$S_{bl} = 0.053 \frac{T^{2.1}}{D_*^{0.3}} \sqrt{(s-1) g D_{50}^3} \quad (1)$$

$$T = \frac{u_*^2 - u_{*cr}^2}{u_{*cr}^2} \quad (2)$$

$$S_{sl} = F \times c_a \times V \times d \quad (3)$$

$$D_* = D_{50} \left[\frac{(s-1) g}{\nu^2} \right]^{1/3} \quad (4)$$

Where S_{bl} is the bed load [m^2/s]; S_{sl} is the suspended load [m^2/s]; T is the non-dimensional transport stage parameter; D_* is the non-dimensional particle parameter; D_{50} is the median particle diameter of be material [m]; $u_*=(g^{0.5}/C')V$ is the bed shear velocity related to flow velocity and roughness; u_{*cr} is the critical bed shear velocity according to Shields; C' is Chézy coefficient, depending on the bottom roughness; V is the average flow velocity [m/s]; s is the specific density of sediment; g is gravitational acceleration [m/s^2]; F is the concentration factor for the suspended load according to the bed load; c_a is the volumetric reference concentration [m^3/m^3] at the reference level a; ν is kinematic viscosity coefficient [m^2/s]; and d is the flow depth [m].

The transport stage parameter (T) is a non-dimensional indicator that measures the excess bed shear stress above the critical threshold, and was calculated according to Eq. 2. In this study, T values typically ranged from 0 to 5, representing conditions from near incipient motion ($T \approx 0$) to strong sediment transport ($T > 1$) (Van Rijn, 1984). Although T is not a directly calibrated parameter, it is derived from flow velocity and sediment properties and thus indirectly influences sediment transport rates.

The erosion coefficient (M), settling velocity (w_s), and critical shear stress (τ_{cr}) are highly site-dependent parameters. In this study, initial reference values were taken from previous sediment transport studies (van Rijn, 1984; Lu et al., 2020; Binh et al., 2022). These values were then adjusted during calibration to match the observed wave and tidal dynamics at the Truong Sa station.

Providing the model with an appropriate mesh size is essential to achieve a reasonable trade-off between accuracy and simulation time. We established the 2D MIKE 21/3 Coupled Model FM with boundaries approximately 1 km northeast, 0.5 km southeast, 0.4 km southwest, and 0.8 km west-northwest from the coral reefs surrounding the island (Fig. 1). The unstructured triangular mesh comprised 854 nodes and 1,419 elements, representing both the nearshore areas and offshore zones (Fig. 3). The finest cell size was 70 m² around the coastline and coral reefs of Truong Sa Island for detailed assessment. In contrast, the largest cell size was 50,000 m² for the offshore areas.

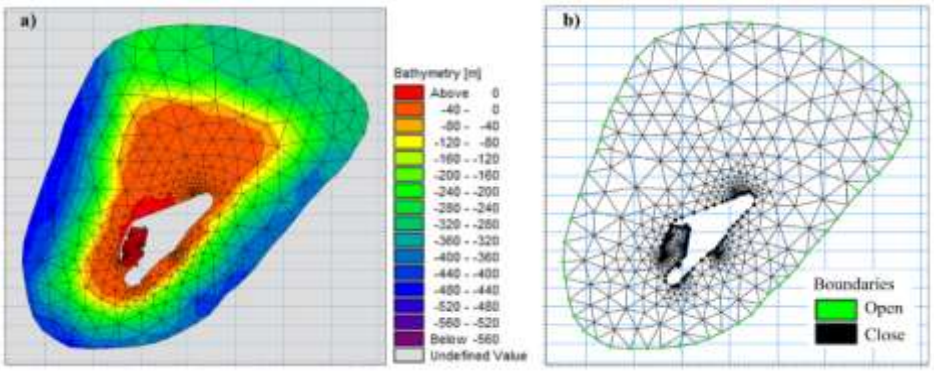

Figure 3. Unstructured triangular mesh of the simulation domain

The open boundary (Fig. 3b) consists of water-level and wave data from the ERA5 reanalysis of the ECMWF (Hersbach et al., 2023), with a 6-hour time interval covering the period from 01 January, 2013, to 31 December, 2018. The 6-hour-interval wind data measured at the Truong Sa Oceanographic station (Fig. 1) were input into the wave module's wind-forcing section. Appendix 3 summarizes the model's boundary conditions. As input conditions for the wave model, we used significant wave height (Hs), wave period (Tp), and wave direction (Dir) from ERA5 at the open boundary. In addition, in-situ Hs and Tp from the Truong Sa station were employed for calibration and validation of the wave module (Appendix 1).

4. Results

4.1. Model calibration and validation

The hydrodynamic and wave modules were calibrated, tested, and validated using water-level and wave data in 2013, 2014, and 2015, respectively, while the sediment transport module was validated using seabed elevation data in 2018. Given the data constraints in this isolated study area, bathymetric data for 2013 were unavailable. Alternatively, the 2010 bathymetry was adopted as the initial condition. We acknowledge that this substitution may introduce considerable uncertainty, especially in dynamically impacted nearshore areas, such as around the Truong Sa Islands. This limitation arises from the lack of synchronous, continuous bathymetric datasets, a common challenge for studies of seabed evolution due to the extremely high cost of bathymetric surveys. Nevertheless, the approach still provides a reasonable first-order assessment of seabed evolution under unfavorable wave conditions.

To assess the model's reliability, we used the Nash-Sutcliffe efficiency (*NSE*) and the coefficient of determination (R^2) as performance metrics. The calibration and validation process involved tuning key numerical and physical parameters, such as

the bed resistance, grain diameter, Manning roughness coefficient, and settling velocity coefficient. The adjustments were made to optimize model performance and improve agreement between simulated and observed data. In total, we ran the model 70 times for model calibration to achieve reasonable results, and the final values of the model parameters are shown in Appendix 4. Our analysis revealed that the wave-breaking coefficient and frequency factor are the most sensitive parameters in the wave module. In the hydrodynamic module, the Manning roughness coefficient had the most significant influence on water-level variations and flow dynamics. To account for spatial variations, we applied a depth-dependent Manning roughness coefficient across the simulation domain, assigning higher values in deeper regions. In the sediment transport module, the settling velocity, along with the erosion and deposition coefficients, was identified during calibration as the key parameters influencing sediment dynamics and bed evolution.

Appendix 5 shows strong agreement between the simulated and observed wave heights and wave directions during the calibration (2013), testing (2014), and validation (2015) phases at the Truong Sa Oceanographic station. For wave height, the *NSE* values are 0.87, 0.86, and 0.87, while the R^2 values are 0.87, 0.86, and 0.90 for calibration, testing, and validation, respectively (Table 1). The maximum simulated wave height in 2013 reached 3.4 m, which was 0.4 m lower (10.5% underestimation) than the observed peak value (Appendix 5A). Similarly, the model shows good agreement in wave direction, though some discrepancies occur at certain times. Simulated wave directions ranged from 0° to 359°, whereas observed values varied from 0° to 315° (Appendix 5B). These results indicate that the wave module achieves a reliable representation of wave dynamics and is suitable for further simulations of the hydrodynamic and sediment transport modules.

Table 1. Results of the model calibration, testing, and validation

Parameter	**Module**	**Calibration (2013)**		**Testing (2014)**		**Validation (2015)**	
		NSE	R^2	*NSE*	R^2	*NSE*	R^2
Wave height	Wave	0.87	0.87	0.86	0.86	0.87	0.90
Water level	Hydrodynamics	0.89	0.90	0.88	0.89	0.88	0.88

Appendix 6 compares the simulated and observed water levels at the Truong Sa Oceanographic station during model calibration (2013), testing (2014), and validation (2015). The results demonstrate a strong agreement between the simulated and observed values in both amplitude and phase variations, with a maximum deviation of only approximately 0.2 m. The *NSE* values for calibration, testing, and validation are 0.89, 0.88, and 0.88, respectively, while the R^2 values are 0.9, 0.89, and 0.88 (Table 1). These results confirm the reliability and accuracy of the hydrodynamic module, supporting its further integration into the sediment transport module.

To validate the sediment transport module, we compared the simulated to the observed seabed elevation data along a transect measured in 2018 (Fig. 1). As shown in Appendix 7, the simulated seabed elevations closely aligned with observations, though the model slightly overestimated elevations in deeper regions. The overall error between the simulated and observed values was approximately 21.6%. Given the complex, highly variable terrain in the study area, where elevations range from -519 m to 2 m, this level of discrepancy falls within an acceptable margin. In conclusion, the coupled wave, hydrodynamic, and sediment transport model demonstrates strong reliability and is well-suited for further analyses.

The study area was divided into four equal quadrants around the Truong Sa Island (Zones 1–4: northeast, southeast, southwest, northwest). This partitioning was applied solely to facilitate comparative analysis of spatial variability in wave dynamics, SSC, and seabed evolution, without reference to specific wind directions or seabed morphology.

4.2. Wave dynamics

Within an 8 km^2 area of the simulation domain, the annual average significant wave height (Hs) between 2013 and 2015 was 0.68 m. Hs were highest in 2015, with an average of 0.78 m, while the lowest was in 2014 at 0.59 m. Figure 4 shows the spatial distribution of Hs, which can be divided into four distinct zones. In Zone 1, the average Hs were 0.87 m, 0.71 m, and 0.65 m in 2015, 2013, and 2014, respectively. Zone 2 exhibited the greatest Hs in 2015 at 0.90 m, followed by a substantial decrease to 0.75 m in 2013 and 0.67 m in 2014. In contrast, Zones 3 and 4 showed relatively stable Hs over the simulation period. Zone 3 had Hs ranging between 0.51 m and 0.67 m, while Zone 4 had values between 0.45 m and 0.62 m. Overall, Zones 1 and 2 experienced higher Hs than Zones 3 and 4 throughout 2013–2015.

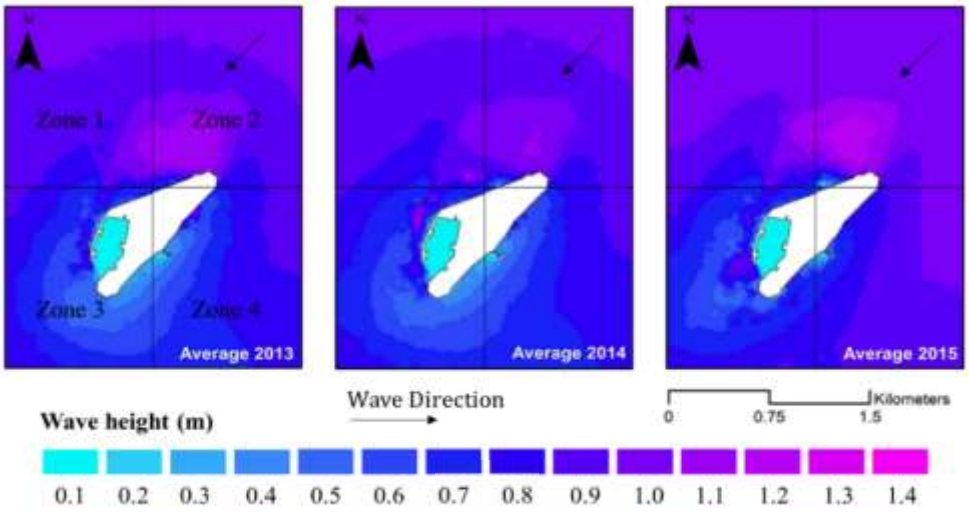

Figure 4. Annual average significant wave heights from 2013 to 2015

Figure 5 shows the seasonal averages of significant wave height (Hs) from 2013 to 2015. Interannually, the Hsin winter (November-April) 2015 was the highest at 1.14 m, followed by 0.98 m in 2014 and 0.71 m in 2013. In summer (May-October), the Hs were relatively stable between 2013 and 2015, ranging from 0.38 m to 0.57 m. Intra-annually, the Hs in winter were higher than in summer during 2013–2015. The patterns above were also consistent across the four zones. Zones 1 and 2 had higher Hs compared to Zones 3 and 4. Particularly, Zone 2 had the highest Hs, averaging 0.8 m during 2013–2015, followed by Zone 1 at 0.77 m. Zone 4 had the lowest average Hs during 2013–2015, at 0.54 m. Seasonally, Zones 2 and 1 had the highest Hs in winter, averaging 1.08 m and 1.01 m from 2013–2015, respectively. The lowest Hs was observed in Zone 3 during the summer of 2013–2015, averaging 0.35 m.

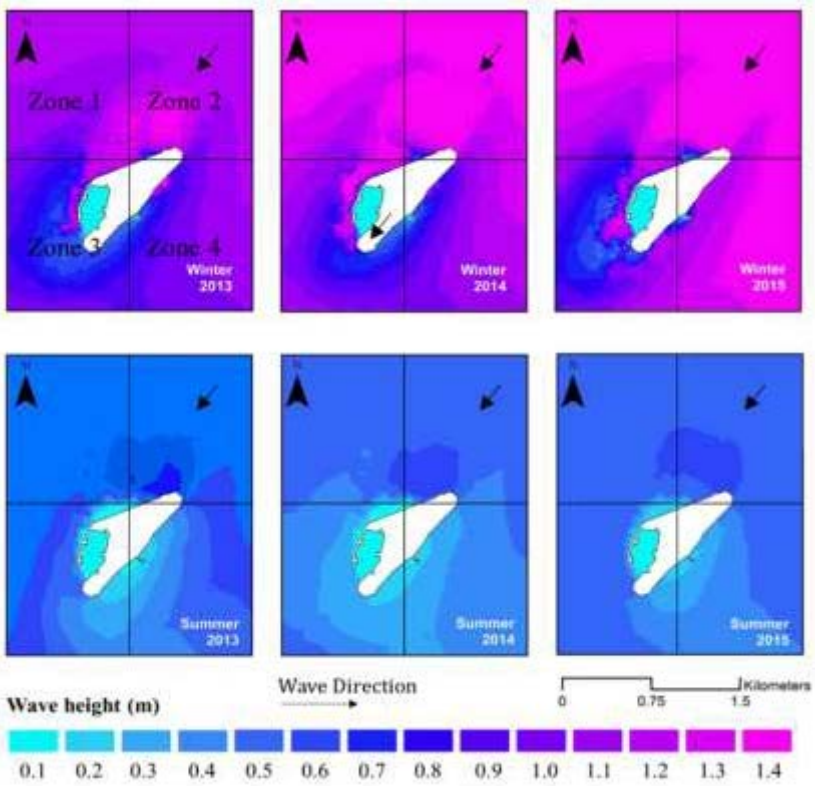

Figure 5. Seasonal significant wave heights from 2013 to 2015

4.3. Suspended sediment dynamics

The annual average SSC in 2015 was the highest among the three studied years (Fig. 6, Appendix 9). The spatially averaged SSC across the entire simulation domain in 2015 was 0.007 g/m^3, higher than 0.004 g/m^3 in 2013 and 0.002 g/m^3 in 2014. In 2015, SSC values exceeding 2.5 g/m^3 were predominant in Zones 2-4. On the other hand, high SSC values concentrated mainly in Zones 1-3 in both 2013 and 2014. SSC values remained low throughout all simulated years in regions farther from the Truong Sa Island.

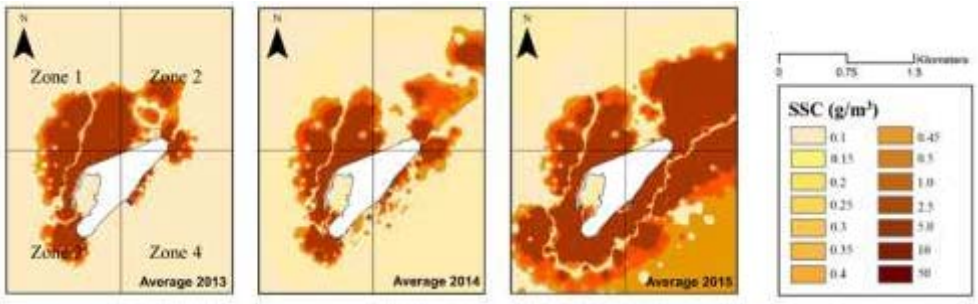

Figure 6. Annual average SSC from 2013 to 2015

Seasonally, the SSC was higher in winter than in summer (Fig. 7). The winter SSC distributions were similar to those of the annual average. In winter 2015, high SSC values were

dominant in Zones 2-4, while in 2013 and 2014, high SSCs were in Zones 1-3. The average SSC in winter 2015 across the entire simulation domain was 0.013 g/m^3, nearly nine times higher than the corresponding value in summer. Similarly, in Zone 4, the average winter SSC in 2015 was 0.019 g/m^3, almost seven times higher than the summer value of 0.003 g/m^3. During summer 2013–2015, high SSCs concentrated primarily in Zones 1-2, whereas Zones 3 and 4 consistently exhibited low SSCs over the study period.

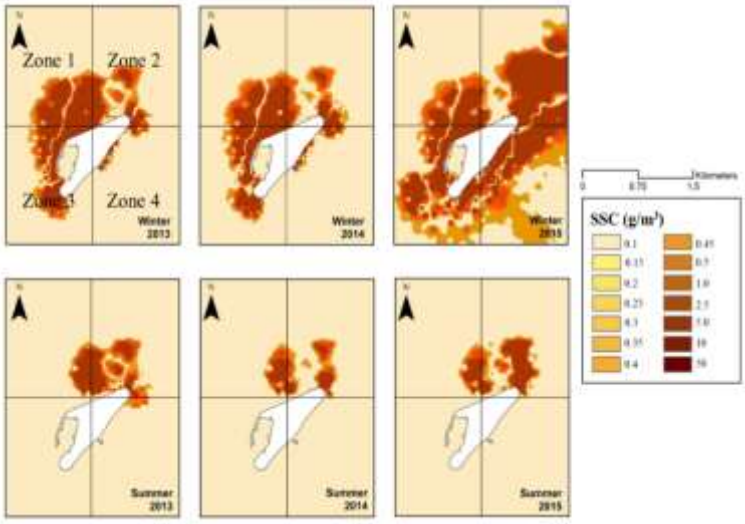

Figure 7. Seasonal SSC variations from 2013 to 2015

4.4. Seabed changes

Figure 8 and Appendix 8 illustrate annual seabed changes from 2013 to 2015, with the most pronounced incision occurring in 2015. Over the whole study area, the total incision volume in 2015 was -1.34 Mm^3, corresponding to an incision depth of -0.54 m. In contrast, the total deposition volume was 1.33 Mm^3, corresponding to a deposition depth of 0.35 m, yielding a net incision volume of -0.12 Mm^3 (-0.19 m incision depth). The spatial distribution of seabed changes in 2015 indicates that 30.7% of the area experienced incision, 47.2% underwent deposition, and 22.1% remained relatively stable (seabed change within 1 mm) (Fig. 9; Appendix 8). Both 2013 and 2014 experienced net deposition, with volumes of 2,576 m^3 in 2013 and 29,621 m^3 in 2014.

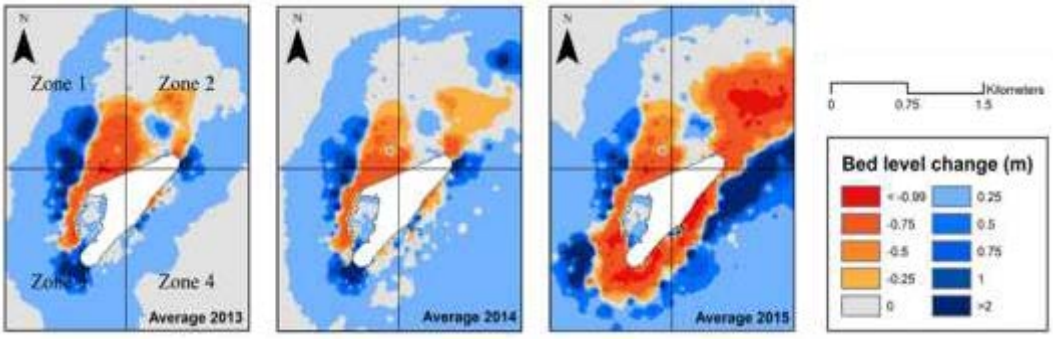

Figure 8. Annual average seabed changes from 2013 to 2015

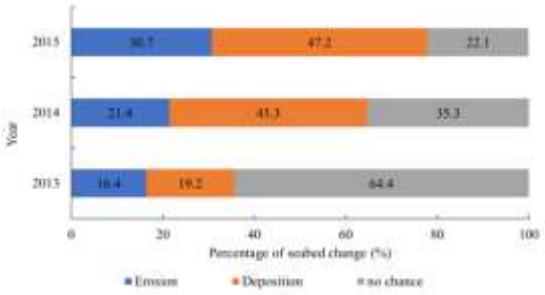

Figure 9. Percentage of the area of the annual average seabed changes in the whole computational domain

Spatially, seabed incision was most significant in Zones 2 and 1, whereas deposition dominated Zones 4 and 3. In Zone 2, the net incision volume was -306,112 m^3 in 2015 (occurring in 64.6% of the area of Zone 2), compared to -127,857 m^3 in 2013 and -43,479 m^3 in 2014. In Zone 1, the net incision was in 2015 (-54,182 m^3, over 23.9% of the area) and 2014 (-35,382 m^3, over 19.4% of the area), whereas the net deposition was in 2013 (19,249 m^3, over 22.1% of the area). Both Zones 4 and 3 experienced a net deposition over the 2013–2015 period. For instance, in 2013, Zone 4 recorded a net deposition volume of 110,471 m^3, accounting for 7.8% of its area.

Seasonally, seabed elevation changes were more dynamic in winter than in summer (Fig. 10). Zone 2 experienced net incision in both seasons throughout 2013–2015. Notably, in winter, net incision volumes were -190,447 m^3 in 2015, compared to -111,223 m^3 in 2013 and -72,679 m^3 in 2014. These seabed incisions accounted for 52.9%, 35.8%, and 34.8% of the total area of Zone 2, respectively. Similarly, Zone 1 was predominantly incised in both 2015 and 2013, whereas in 2013 it underwent net deposition in both seasons. For instance, the net incision volume in winter 2015 was -47,016 m^3. On the other hand, both Zones 4 and 3 experienced net depositions in winter and remained relatively stable in summer. In winter 2015, the net deposition of Zone 4 was 58,190 m^3.

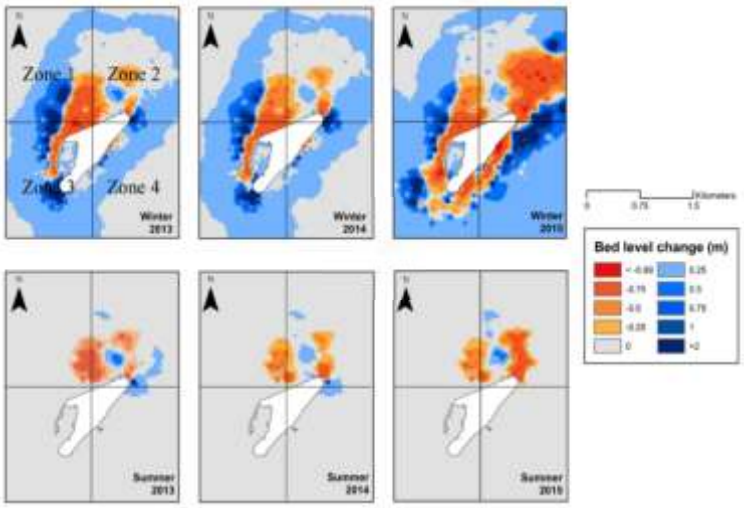

Figure 10. Seasonal seabed changes from 2013 to 2015

5. Discussions

5.1. Seabed dynamics and suspended sediment response

The simulated results indicate that seabed incision predominantly occurred near the shoreline of the Truong Sa Island (Fig. 8, Appendix 8), particularly in Zone 2, where a net incision of up to -306,112 m^3 was observed over 64.6% of the area in 2015. Such pronounced seabed changes may elevate coastal erosion risks and threaten the

livelihoods of local communities. These incisions increase coastal areas' vulnerability to storms, wave action, and erosion, potentially compromising the natural protections on which local communities rely (Yates et al., 2017).

To mitigate such risks, sediment nourishment can be an effective measure. The dredged sediment can be replenished in the protective beaches to maintain the coastal integrity. Although effective, sediment nourishment may need periodic re-nourishment to support its effectiveness, for example, every 2 or 5 years, depending on the nourishment scale (Adell et al., 2024; Saengsupavanich et al., 2023). Additionally, nature-based solutions (e.g., revegetation) are emerging as having long-term positive effects on coastal stability, supporting coastal communities (Yasmeen et al., 2024).

5.2. Implications for coral reef ecosystems

The coral reef region (Fig. 1) around the Truong Sa Island was highly affected by seabed incision (Figs. 11, 12). This erosional dominance is similar to other coral reefs; for instance, Yates et al. (2017) found that 77% of the five studied coral reef systems (60 individual reefs) in the Atlantic, Pacific, and Caribbean have been eroded over the past several decades.

In addition to seabed changes, strong waves may also pose a direct and serious threat to coral reef ecosystems. High SSCs induced by wave-driven resuspension increase turbidity, reducing light penetration and consequently inhibiting coral photosynthesis and growth (Pomeroy et al., 2021). Strong wave events may also resuspend fine sediments enriched with organic matter and pollutants, leading to hypoxia and the release of harmful substances that stress or kill corals, thereby contributing to environmental degradation (Weber et al., 2012). Therefore, in addition to accelerating seabed incision, strong waves create persistent turbidity and potential contamination, undermining coral reef health, reducing biodiversity, and degrading critical ecosystem services in the Truong Sa region.

5.3. Implications for island management and navigation

Waves in winter are strong, making ship navigation difficult. In that regard, Zones 3 and 4 can be used for ship docking areas under moderate waves (in 2013 and 2014). However, during stronger waves (in 2015), ship docking in Zone 4 may become risky, while Zone 3 remains safe. Throughout the three studied years, waves in Zones 1 and 2 were strong, reaching heights of up to 1.4 m, which may create a dangerous environment for ship navigation and fishing activities, especially for small and moderate ships and boats. In contrast, waves were low in the summer of all examined years, thus suitable for ship navigation and fishing. Similar to the winter, the summer waves in Zones 3 and 4 (with wave heights mostly less than 0.5 m) were not as strong as those in Zones 1 and 2 (with wave heights of up to 0.8 m).

5.4. Study limitations and future directions

The simulated results provide insights into wave-induced seabed changes and suspended sediment dynamics, having significant implications for island management, ship navigation, and coral reef conservation. However, the current research still has some limitations.

A key limitation of this study is the reliance on the 2010 bathymetry as the initial condition and the 2018 bathymetry for validation. This temporal mismatch can introduce significant errors in estimates of seabed evolution. Due to data constraints, we were unable to conduct a sensitivity or quantitative analysis of how these input uncertainties may influence the model results.

Moreover, the lack of in situ SSC observations hindered validation of the

sediment module. While satellite remote sensing has been widely used to estimate SSC in nearshore and estuarine regions, extracting reliable SSC information in offshore island environments remains very challenging due to water depth, atmospheric effects, and cloud cover. However, this represents a promising direction for improving the model by integrating multi-source remote sensing data.

Another limitation is the absence of a regional sediment budget analysis, which reduces the precision of inferred connections between wave–current interactions, SSC, and seabed erosion/accretion. Including this analysis in future studies will provide more substantial evidence of sediment pathways and mass balance.

Finally, additional hydrodynamic processes such as coastal currents, breaking waves, and tidal effects were not explicitly considered in the simulations. Although waves are the dominant driver of sediment transport, these processes could further refine the understanding of seabed evolution and ecological impacts.

Collectively, while these limitations constrain the model's precision, the study provides valuable insights into the wave-driven sediment dynamics of Truong Sa Island, offering a foundation for future integrated management and ecosystem protection strategies.

6. Conclusions

Located in a strategically important region for global maritime trade, the sustainable development of islands in the Truong Sa Archipelago remains a critical issue yet has received less attention, likely due to the scarcity of reliable observational data. In this study, we examined suspended sediment dynamics and seabed morphological changes surrounding the Truong Sa Island under strong wave conditions over a continuous three-year period from 2013 to 2015.

Simulation results revealed that seabed changes were most pronounced in nearshore areas, driven primarily by prevailing wave conditions. Nearshore zones experienced significant seabed incision and elevated suspended sediment concentrations, while offshore areas remained relatively stable. Seasonal variations were observed, with more substantial seabed changes and higher suspended sediment concentrations occurring during winter months. The southwest harbor showed potential for deposition, suggesting the need for management measures, such as dredging, to maintain navigational efficiency. These patterns highlight the critical links between wave dynamics, sediment transport, and ecological and socio-economic impacts in the Truong Sa region.

The findings contribute to the current understanding of wave-driven sediment dynamics and provide practical insights for island management, navigation safety, and coral reef conservation. Compared with previous studies, this work emphasizes the spatial variability of sediment responses and identifies areas requiring targeted interventions. Despite limitations stemming from reliance on historical bathymetry and the lack of in situ sediment observations, the study establishes a foundation for future research. Future work should integrate comprehensive datasets, including multi-source remote sensing, in-situ measurements, and additional hydrodynamic processes such as coastal currents, tides, and breaking waves, to improve model accuracy and support evidence-based strategies for sustainable island management and long-term protection of marine ecosystems.

Acknowledgements

This study is funded by the Institute of Earth Sciences, VAST, under grant number CSCL24.02/24-25; VAST05.01/24-25.

References

Adell A., Kroon A., Almström B., Larson M., Hallin C., 2024. Observed beach nourishment development in a semi-enclosed coastal embayment. Geomorphology, 462, 109324.

Bacmeister J.T., Reed K.A., Hannay C., Lawrence P., Bates S., Truesdale J.E., Rosenbloom N., Levy M., 2018. Projected changes in tropical cyclone activity under future warming scenarios using a high-resolution climate model. Climatic Change, 146(3), 547–560.

Barnett J., Adger W.N., 2003. Climate Dangers and Atoll Countries. Climatic Change, 61(3), 321–337.

Binh D.V., Wietlisbach B., Kantoush S., Loc H.H., Park E., Cesare G.D., Cuong D.H., Tung N.X., Sumi T., 2020. A Novel Method for River Bank Detection from Landsat Satellite Data: a case study in the Vietnamese Mekong Delta, Remote Sensing, 12(20), 3298.

Bramante J.F., Ashton A.D., Storlazzi C.D., Cheriton O.M., Donnelly J.P., 2020. Sea Level Rise Will Drive Divergent Sediment Transport Patterns on Fore Reefs and Reef Flats, Potentially Causing Erosion on Atoll Islands. Journal of Geophysical Research: Earth Surface, 125(10), e2019JF005446.

Campbell J.R., 2018. Climate Change Impacts on Atolls and Island Nations in the South Pacific. In: D.A. Dellasala and M.I. Goldstein (Editors), Encyclopedia of the Anthropocene, 2, 227-232. https://doi.org/10.1016/B978-0-12-809665-9.09772-X.

Dang Nguyen H., Trung Ngo D., Viet Vu D., 2023. Benthic habitat mapping and assessment of seagrass species diversity in Da Lon Reef, Truong Sa Islands, Vietnam, using very high-resolution satellite imagery and in situ data. Vietnam Journal of Earth Sciences, 45(4), 531–552. https://doi.org/10.15625/2615-9783/19026.

DHI, 2014. MIKE 21/3 Coupled Model FM: User guide.

Ford M., Merrifield M.A., Becker J.M., 2018. Inundation of a low-lying urban atoll island: Majuro, Marshall Islands. Natural Hazards, 91(3), 1273–1297.

Friedlander A.M., 2018. Marine conservation in Oceania: Past, present, and future. Marine Pollution Bulletin, 135, 139–149.

Han D.H.T., James D., Waheed Z., Phua M.-H., 2024. THREE-DECADE changes of reef cover in Pulau Layang-Layang, Malaysia using multitemporal Landsat images. Marine Environmental Research, 197, 106454.

Hanich Q., Wabnitz C.C.C., Ota Y., Amos M., Donato-Hunt C., Hunt A., 2018. Small-scale fisheries under climate change in the Pacific Islands region. Marine Policy, 88, 279–284.

Hersbach H., Bell B., Berrisford P., Biavati G., Horányi A., Muñoz Sabater J., Nicolas J., Peubey C., Radu R., Rozum I., Schepers D., Simmons A., Soci C., Dee D., Thépaut J-N., 2023. ERA5 hourly data on single levels from 1940 to present. Copernicus Climate Change Service (C3S) Climate Data Store (CDS). Doi: 10.24381/cds.adbb2d47.

Holdaway A., Ford M., Owen S., 2021. Global-scale changes in the area of atoll islands during the 21st century. Anthropocene, 33, 100282.

Huang D., Licuanan W.Y., Hoeksema B.W., Chen C.A., Ang P.O., Huang H., Lane D.J.W., Vo S.T., Waheed Z., Affendi Y.A., Yeemin T., Chou, L.M., 2015. Extraordinary diversity of reef corals in the South China Sea (East Sea). Marine Biodiversity, 45(2), 157–168.

Kench P.S., Mann T., 2017. Reef Island Evolution and Dynamics: Insights from the Indian and Pacific Oceans and Perspectives for the Spermonde Archipelago. Frontiers in Marine Science, 4, 145.

Kench P.S., Ford M.R., Bramante J.F., Ashton A.D., Donnelly J.P., Sullivan R.M., Toomey M.R., 2022. Heightened storm activity drives late Holocene reef island formation in the central Pacific Ocean. Global and Planetary Change, 215, 103888.

Kennedy D.M., 2024. A review of the vulnerability of low-lying reef island landscapes to climate change and ways forward for sustainable management. Ocean & Coastal Management, 249, 106984.

Kokelaar B.P., Durant G.P., 1983. The submarine eruption and erosion of Surtla (Surtsey), Iceland. Journal of Volcanology and Geothermal Research, 19(3–4), 239–246.

Li J., Wang Y.P., Gao S., 2024. In situ hydrodynamic observations on three reef flats in the Nansha Islands,

South China Sea (East Sea). Frontiers in Marine Science, 11, 1375301.

Khuong V.L., Le V.T., Hoang V.T., Nguyen Đình H., Do V.M., 2022. Characteristics and transformation of seabed topography in Truong Sa Island area . Journal of Geodesy and Cartography, (53), 9–17. https://doi.org/10.54491/jgac.2022.53.650.

Lu X., Wang X., Ban X., Singh V.P., 2020. Transport characteristics of non-cohesive sediment with different hydrological durations and sediment transport formulas. Journal of Hydrology, 591, 125489.

Lyons M., Phinn S., Roelfsema C., 2011. Integrating Quickbird Multi-Spectral Satellite and Field Data: Mapping Bathymetry, Seagrass Cover, Seagrass Species and Change in Moreton Bay, Australia in 2004 and 2007, Remote Sensing, 3(1), 42–64.

Lyons M.B., Roelfsema C.M., Kennedy E.V., Kovacs E.M., Borrego-Acevedo R., Markey K., Roe M., Yuwono D.M., Harris D.L., Phinn S.R., Asner G.P., Li J., Knapp D.E., Fabina N.S., Larsen K., Traganos D., Murray N.J., 2020. Mapping the world's coral reefs using a global multiscale earth observation framework. Remote Sensing in Ecology and Conservation, 6(4), 557–568.

Ma Y., Jiang C., Li S., Liu Y., Wen X., Long Y., Yuan S., Kang Y., Wang Y., Wu R., 2023. Ecological vulnerability assessment of coral islands and reefs in the South China Sea (East Sea) based on remote sensing and reanalysis data. Frontiers in Ecology and Evolution, 11, 1066961.

Martyr-Koller R., Thomas A., Schleussner C.-F., Nauels A., Lissner T., 2021. Loss and damage implications of sea-level rise on Small Island Developing States. Current Opinion in Environmental Sustainability, 50, 245–259.

Mentaschi L., Vousdoukas M.I., Pekel J.-F., Voukouvalas E., Feyen L., 2018. Global long-term observations of coastal erosion and accretion. Scientific Reports, 8(1), 12876.

Mora C., Caldwell I.R., Birkeland C., McManus J.W., 2016. Dredging in the Spratly Islands: Gaining Land but Losing Reefs. PLOS Biology, 14(3), e1002422.

Nguyen Dang H., Ngo Trung D., Kuznetsov A., Vu Le P., 2022. Classification and mapping of marine-island landscape in Nam Yet Island, Truong Sa Islands, Vietnam. Vietnam Journal of Earth Sciences, 44(4), 481–501. https://doi.org/10.15625/2615-9783/17178.

Nguyen X.H., Dinh V.U., Mai V.K., Tran V.T., Pham V.T., 2017. Impacts of climate change on wave regimes in the East Sea. Vietnam Journal of Science, Technology and Engineering, 59(1), 88–92.

Pomeroy A.W.M., Storlazzi C.D., Rosenberger K.J., Lowe R.J., Hansen J.E., Buckley M.L., 2021. The Contribution of Currents, Sea-Swell Waves, and Infragravity Waves to Suspended-Sediment Transport Across a Coral Reef-Lagoon System. Journal of Geophysical Research: Oceans, 126(3), e2020JC017010.

Saengsupavanich C., Pranzini E., Ariffin E.H., Yun L.S., 2023. Jeopardizing the environment with beach nourishment. Science of The Total Environment, 868, 161485.

Smith L., Cornillon P., Rudnickas D., Mouw C.B., 2019. Evidence of Environmental Changes Caused by Chinese Island-Building. Scientific Reports, 9(1), 5295.

Storlazzi C.D., Gingerich S.B., van Dongeren A., Cheriton O.M., Swarzenski P.W., Quataert E., Voss C.I., Field D.W., Annamalai H., Piniak G.A., McCall R., 2018. Most atolls will be uninhabitable by the mid-21st century because of sea-level rise exacerbating wave-driven flooding. Science Advances, 4(4), eaap9741.

The Nature Conservancy, 2009. Indicators of Hydrologic Alteration Version 7.1 User's Manual.

van Rijn L.C., 1984. Sediment transport, Part II: Suspended load transport. Journal of Hydraulic Engineering, 110(11), 1613–1641.

Vousdoukas M.I., Athanasiou P., Giardino A., Mentaschi L., Stocchino A., Kopp R.E., Menéndez P., Beck M.W., Ranasinghe R., Feyen L., 2023. Small Island Developing States under threat by rising seas even in a 1.5°C warming world. Nature Sustainability, 6(12), 1552–1564.

Vu T.H., Binh D.V., Tran H.N., Khan M.A., Bui D.D., Stamm J., 2024. Quantifying spatio-temporal river morphological change and its consequences in the Vietnamese Mekong River Delta using remote

sensing and geographical information system techniques. Remote Sensing, 16(4), 707.

Vu V.-T., Vu M.-C., 2024. 3D bathymetric images of the Truong Sa Archipelago (Spratly Islands). Regional Studies in Marine Science, 73, 103509.

Watson S.J., Whittaker J.M., Lucieer V., Coffin M.F., Lamarche G., 2017. Erosional and depositional processes on the submarine flanks of Ontong Java and Nukumanu atolls, western equatorial Pacific Ocean. Marine Geology, 392, 122–139.

Weber M., de Beer D., Lott C., Polerecky L., Kohls K., Abed R.M.M., Ferdelman T.G., Fabricius K.E., 2012. Mechanisms of damage to corals exposed to sedimentation. Proceedings of the National Academy of Sciences, 109(24), E1558–E1567.

Wolanski E., Choukroun S., Nhan N.H., 2020. Island building and overfishing in the Spratly Islands archipelago are predicted to decrease larval flow and impact the whole system. Estuarine, Coastal and Shelf Science, 233, 106545.

Yasmeen A., Pumijumnong N., Arunrat N., Punwong P., Sereenonchai S., Chareonwong U., 2024. Nature-based solution for coastal erosion protection in the muddy coasts: Empirical perceptibility from the Upper Gulf of Thailand. Ocean & Coastal Management, 259, 107488.

Yates K.K., Zawada D.G., Smiley N.A., Tiling-Range G., 2017. Divergence of seafloor elevation and sea level rise in coral reef ecosystems. Biogeosciences, 14(6), 1739–1772.

Yen P.Q., Hoai D.K., Hoa D.T.B., 2017. Research bathymetry mapping of shallow water areas around islands in the Truong Sa Archipelago by deep - remote sensing technology. VNU Journal of Science: Earth and Environmental Sciences, 33(4), 63–73.

APPENDIX

Appendix 1. Summary of datasets used in this study

Data type	Source	Period	Temporal resolution	Spatial resolution	Role in the model	Notes
Wave (height (Hs), period (Tp), and direction (Dir))	VAST - Truong Sa station	2005–2022	Daily	Point (station)	Calibration, validation, and extreme wave analysis	In-situ
Wave (Hs, Tp, Dir)	ERA5 ECMWF	2013–2018	6-hour	0.25° (~25 km)	Boundary condition for the wave module	Offshore forcing
Wind speed & direction	VAST - Truong Sa station	2013–2018	6-hour	Point (station)	Local forcing in the wave module	In-situ
Wind (U10)	ERA5 ECMWF	2013–2018	6-hour	0.25° (~25 km)	Supplementary comparison with in-situ measurements	Validation
Water level	VAST - Truong Sa gauge	2013–2015	12-hour	Point (station)	Calibration, validation of the hydrodynamic model	In-situ
Water level	ERA5 ECMWF	2013–2018	6-hour	0.25° (~25 km)	Boundary condition for the hydrodynamic model	Offshore
Bathymetry	VAST	2010	Point (100 m spacing)		Model geometry	Single-beam echo sounder, ±0.1 m
Bathymetry	VAST	2018	Point (300 m spacing)		Validation	Multibeam echo sounder, ±0.05 m

Appendix 2. Annual 1-day and 90-day wave height maxima from 2005 to 2022

Year	1-day max (m)	90-day max (m)	Year	1-day max (m)	90-day max (m)
2005	3.83	0.99	2014	3.83	1.20
2006	4.00	1.23	2015	3.5.0	1.31
2007	5.33	1.11	2016	3.17	0.97
2008	3.33	1.19	2017	3.75	0.77
2009	3.67	1.22	2018	3.67	1.16
2010	3.83	1.17	2019	2.67	0.84
2011	4.00	1.26	2020	3.17	0.976
2012	3.00	1.13	2021	3.33	1.01
2013	3.67	1.35	2022	2.33	0.75

Appendix 3. Model forcing and boundary conditions used in the MIKE 21/3 coupled model

Component	Type / Purpose	Data source	Temporal resolution	Spatial resolution	Period	Notes
Water level	Open boundary condition	ERA5 reanalysis - ECMWF	6-hour	0.5 × 0.5°	2013–2015	Applied at the open sea boundaries for water level forcing
Wind forcing	Surface forcing (for wave & Hydrodynamics)	Truong Sa Oceanographic Station - VAST	6-hour	Point source	2013–2015	Used to simulate wind-induced surface flow and wave generation
Wave boundary	Spectral wave boundary condition	ERA5 spectral wave data - ECMWF	6-hour	0.5 × 0.5°	2013–2015	Used in wave module for incoming wave spectra
Bathymetry	Initial seabed condition	VAST (2010 data)	-	100 m (point spacing)	-	Interpolated to model grid as initial condition for bed evolution

Appendix 4. Final numerical and physical values of the validated model

Parameters	Module	Value	Unit
Manning roughness coefficient	Hydrodynamics	0.015–0.05	$s/m^{1/3}$
Time weight of the gravity component in the momentum equation	Hydrodynamics	0.5	-
Number of sediment fraction	Sediment transport	1	-
Number of bed layer	Sediment transport	2	-
Active layer	Sediment transport	0.05	m
Median grain diameter	Sediment transport	$0.03.10^{-3}$	m
Calculation time step	Sediment transport	60	s
Settling velocity	Sediment transport	0.03	m/s
Critical shear stress for deposition	Sediment transport	0.01	N/m^2
Erosion coefficient	Sediment transport	5.10^{-7}	$kg/m^2/s$
Critical shear stress for erosion	Sediment transport	1.8	N/m^2
Density of bed layer	Sediment transport	1,550	kg/m^3
Erosion coefficient (M)	Sediment transport	1×10^{5}	$kg/m^2/s$
Number of frequencies	Wave	25	-
Minimum frequency	Wave	0.055	hz
Frequency factor	Wave	1.1	-
Wave breaking coefficient	Wave	0.8	-
Bottom friction coefficient (Nikuradse)	Wave	0.038	m
Cdis coefficient	Wave	4.5	-
DELTA coefficient	Wave	0.5	-

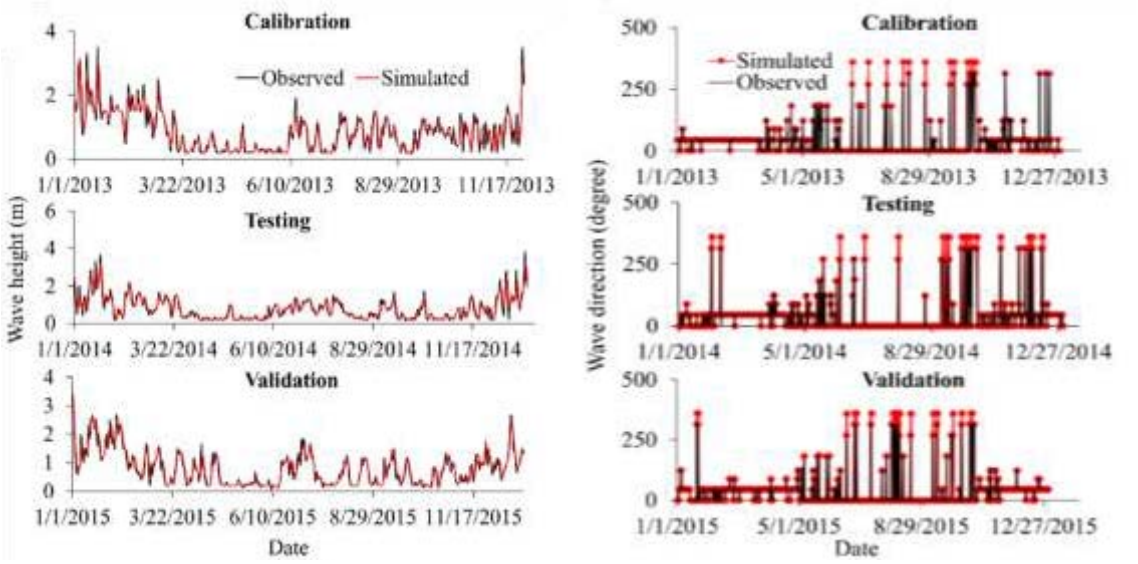

A **B**

Appendix 5. Simulated versus observed wave height (A) and wave direction (B) at the Truong Sa Oceanographic station for model calibration, testing, and validation

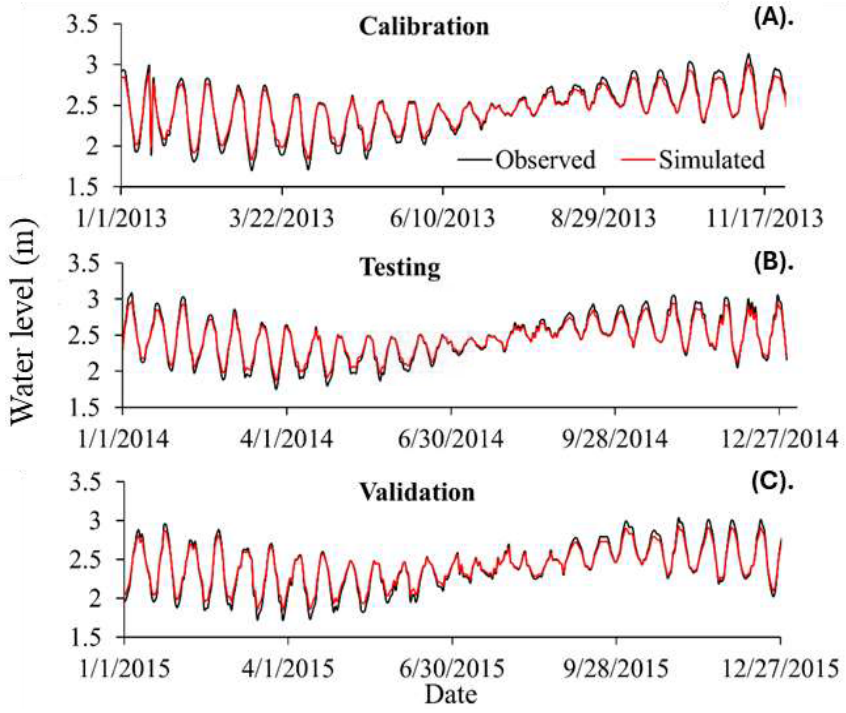

Appendix 6. Simulated versus observed water levels at the Truong Sa Oceanographic station for (A) Model calibration, (B) testing, and (C) validation

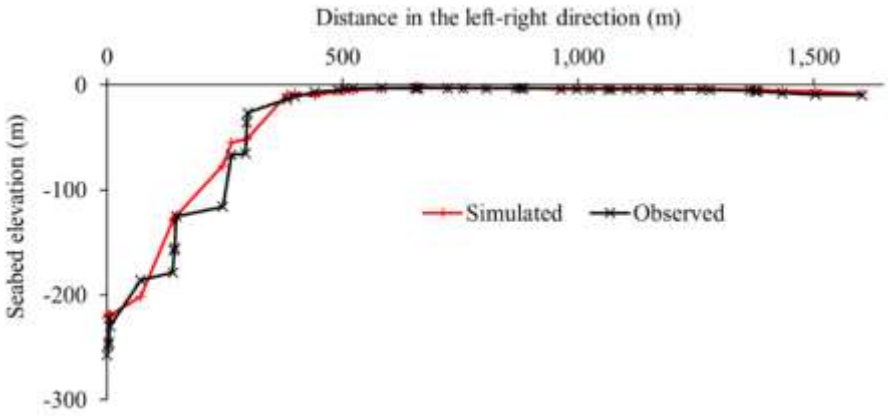

Appendix 7. Simulated versus observed seabed elevations along a transect in 2018, which is shown in Fig. 1

Appendix 8. Annual seabed changes in total volume, average depth, total affected area, and percentage of total affected area from erosion and deposition in the whole simulation domain from 2013 to 2015

Annual seabed changes in	Year	Erosion	Deposition	No change	Net change
Total volume (10^3 m^3)	2013	–439.7	442.3	-	2.6
	2014	–438.9	468.5	-	29.6
	2015	–1,342.4	1,330.2	-	–12.2
Average depth (m)	2013	–0.33	0.29	-	–0.04
	2014	–0.25	0.13	-	–0.12
	2015	–0.54	0.35	-	–0.19
Total affected area (km^2)	2013	1.3	1.5	5.2	0.2
	2014	1.7	3.5	2.8	1.8
	2015	2.5	3.8	1.8	1.3
Percentage of total affected area (%)	2013	16.4	19.2	64.4	-
	2014	21.4	43.3	35.3	-
	2015	30.7	47.2	22.1	-

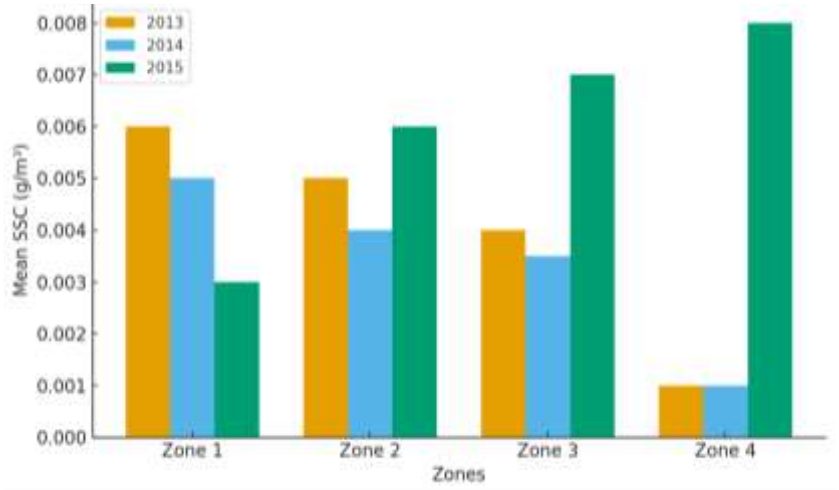

Appendix 9. Chart of annual average SSC from 2013 to 2015 Chart